Biochemical Pharmacology xxx (xxxx) xxx

Contents lists available at ScienceDirect

Biochemical Pharmacology

journal homepage: www.elsevier.com/locate/biochempharm

Metformin-conjugated micellar system with intratumoral pH responsive de-shielding for co-delivery of doxorubicin and nucleic acid

Yanhua Liu [1,2], Jingjing Sun [2], Yixian Huang, Yichao Chen, Jiang Li, Lei Liang, Jieni Xu, Zhuoya Wan, Bei Zhang, Zuojun Li, Song Li [*]

Center for Pharmacogenetics, Department of Pharmaceutical Sciences, School of Pharmacy, University of Pittsburgh, Pittsburgh, PA 15261, United States

ARTICLE INFO

Keywords:
PMet-P(cdmPEG$_{2K}$) micelles
IL-12 cytokine gene
DOX
Intratumor pH responsive
siRNA delivery

ABSTRACT

A novel PMet-P(cdmPEG$_{2K}$) polymeric micellar carrier was developed for tumor-targeted co-delivery of DOX and nucleic acids (NA), based on polymetformin and a structure designed to lose the PEG shell in response to the acidic extracellular tumor environment. NA/DOX co-loaded micelleplexes exhibited enhanced inhibition of cell proliferation compared to DOX-loaded micelles, and displayed a higher level of cytotoxicity at an acidic pH (6.8) which mimicks the tumor microenvironment. The PMet-P(cdmPEG$_{2K}$) micelles achieved significantly improved transfection with either a reporter plasmid or Cy3-siRNA, and enhanced DOX intracellular uptake in 4T1.2 cells at pH 6.8. Importantly, PMet-P(cdmPEG$_{2K}$) micelles showed excellent pEGFP (EGFP expression plasmid) transfection in an aggressive murine breast cancer (4T1.2) model. By using a plasmid encoding *IL-12* (pIL-12), we investigated the combined effect of chemotherapy and gene therapy. PMet-P(cdmPEG$_{2K}$) micelles co-loaded with DOX and pIL-12 were more effective at inhibiting tumor growth compared to micelles loaded with DOX or pIL-12 alone. In addition, this micellar system was effective in co-delivery of siRNA and DOX into tumor cells. Our results suggest that PMet-P(cdmPEG$_{2K}$) has the potential for chemo and nucleic acid combined cancer therapy.

1. Introduction

Recent advancement in cancer genome research has led to the discovery of many genes as novel therapeutic targets for cancer treatment [1]. However, some targets are deemed "undruggable" due to the large interfaces of protein–protein interaction (PPI) or unmatched protein pockets [2,3]. Gene therapy, which employs nucleic acid-based therapeutics (including DNA and RNA) represents an attractive approach [4–6]. In spite of high selectivity, the effectiveness of gene therapy is limited by significant barriers including enzymatic degradation and poor cellular uptake [7,8]. Both viral and non-viral vectors have been developed to protect and deliver nucleic acids [9]. Strategies for combining gene therapy with standard chemotherapy also holds considerable promise for improving the therapeutic efficacy [10,11]. However, effective in vivo co-delivery of chemotherapeutic agents and nucleic acids is particularly challenging due to the differences in physicochemical properties of the two types of agents [12,13].

A variety of cationic polymeric micelles have been explored as carriers for co-delivery of chemotherapeutic drugs and genes in vitro and in vivo [4,14–17]. One challenge is that highly positively charged micelles are prone to interact with serum components in blood, leading to severe aggregation and rapid clearance from the blood circulation by the reticuloendothelial system [18,19]. PEGylation of cationic polymeric micelles has been proven to be an effective strategy to sterically stabilize micelles and minimize the nonspecific interaction in vivo, thus prolonging the circulation time. This facilitates tumor accumulation via the enhanced permeation and retention (EPR) effect [20–22]. However, PEGylation can also markedly reduce cellular uptake in tumor tissues, thus limiting the efficiency of intracellular delivery [23,24]. To circumvent the negative effects of PEGylation on cellular uptake, several PEG shielding/de-shielding strategies have been developed to introduce a PEG shell that functions as a carrier in the circulation but is detached upon reaching the target tissues [25,26]. Carboxydimethyl maleate (cdm) is an acid-labile linker which can be cleaved at a pH characteristic

* Corresponding author.
E-mail address: sol4@pitt.edu (S. Li).
[1] The current address of Yanhua Liu is Department of Pharmaceutics, School of Pharmacy, Ningxia Medical University, No. 1160, Shengli Street, Yinchuan 750004, China.
[2] Yanhua Liu and Jingjing Sun made an equal contribution in this work.

https://doi.org/10.1016/j.bcp.2021.114453
Received 11 November 2020; Received in revised form 23 January 2021; Accepted 26 January 2021
Available online 3 February 2021

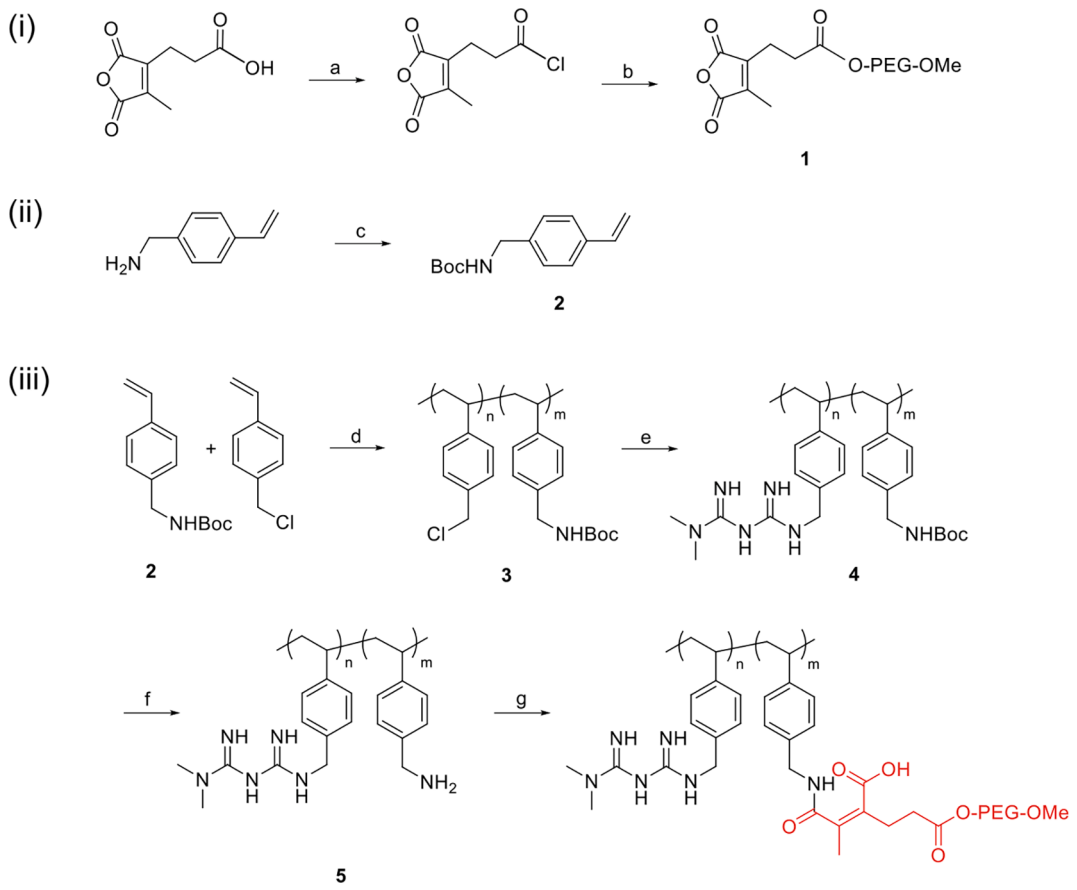

Scheme 1. Synthesis scheme of PMet-P(cdmPEG$_{2K}$) polymer. a) cdm, oxalyl chloride, DMF, rt, 1 h; b) monomethoxy PEG$_{2K}$, DCM, rt, 24 h; c) Boc$_2$O, TEA, MeOH, rt, 24 h; d) AIBN, 4-Cyano-4-[(dodecylsulfanylthiocarbonyl) sulfanyl] pentanoic acid, THF, 90 °C, 24 h; e) MET, DIPEA, DMSO, 110 °C, 48 h; f) TFA, DMSO, rt, 2 h; g) Compound 2, DMSO, 37 °C, 24 h.

of the tumor microenvironment (pH = 6.5–6.8) [27]. Based on the differences in extracellular pH between normal tissues (pH = 7.4) and tumor tissues (pH = 6.5–7.2), conjugation of the cationic polymers with PEG chains via a cdm linker has become an effective strategy to construct pH-responsive PEG detachable carriers for improved tumor-selective delivery of drugs and genes, and the subsequent step of cellular internalization [28,29]. However, there are few reports concerning the in vivo co-delivery of chemotherapeutic drugs and genes using PEG-detachable cationic micelles.

In this work, a novel metformin (dimethybiguanide, Met)-based and cdm-linked cationic micellar carrier PMet-P(cdmPEG$_{2K}$) with PEG deshielding characteristics was developed for co-loading and tumor-targeted co-delivery of the chemotherapeutic drug doxorubicin (DOX) and nucleic acids. Metformin is a commonly used antidiabetic drug for treatment of type II diabetes [30–32]. Increasing evidence demonstrates that Met also has potent antitumor activity against different cancers, which is primarily attributed to the activation of adenosine monophosphate-activated protein kinase (AMPK), and to inhibition of the mammalian target of rapamycin (mTOR) [30]. Moreover, the biguanide group of Met can be used as an ideal cationic motif for constructing gene delivery carriers [33,34]. We synthesized and characterized the PMet-P(cdmPEG$_{2K}$) polymer for co-delivery of DOX and an interleukin-12 (IL-12) expression plasmid. The effectiveness of PMet-P (cdmPEG$_{2K}$) in tumor-selective co-delivery of DOX and siRNA also was investigated.

2. Materials and methods

2.1. Materials

Doxorubicin hydrochloride (DOX·HCl) was purchased from LC Laboratories, MA, USA [35]. 4-Vinylbenzyl chloride, 4-cyano-4-[(dodecylsulfanylthiocarbonyl) sulfanyl] pentanoic acid, 2-azobis(isobutyro nitrile) (AIBN), N, N-diisopropylethylamine, metformin hydrochloride, monomethoxy PEG$_{2K}$, branched and linear polyethyleneimine (PEI, MW = 25 kDa), dulbecco's modified eagle's medium (DMEM), trypsin-EDTA solution, 3-(4,5-dimethylthiazol-2-yl)-2,5-diphenyl tetrazolium bromide (MTT), triton X-100, hoechst 33342, lysotracker Green DND-26, FAM-labeled siRNA and AF647-labeled siRNA were all purchased from Sigma-Aldrich, MO, USA. Penicillin-streptomycin solution and fetal bovine serum (FBS) were purchased from Invitrogen Life Technologies (Gaithersburg, MD, USA). 4-Vinylbenzylamine, 2-propionic-3-methylmaleic anhydride (cdm) were obtained from TCI, PA, USA. All other reagents were of analytical or chromatographic grade.

EGFP expression plasmid (pEGFP) and luciferase expression plasmid (pLuc) were propagated in competent Escherichia coli DH5α cells. pIL-12 and control pDNA were kindly provided by Dr. Shulin Li at MD Anderson Cancer Center, USA. All endotoxin-free plasmids were prepared using the endotoxin free Plasmid Maxiprep Kit according to the manufacturer's instructions.

2.2. Synthesis and characterization of PMet-P(cdmPEG$_{2K}$) polymer

2.2.1. Synthesis of PEG$_{2K}$-cdm and Boc-protected 4-vinylbenzylamine

PEG$_{2K}$-cdm (**compound 1,** Scheme 1) and the Boc-protected 4-

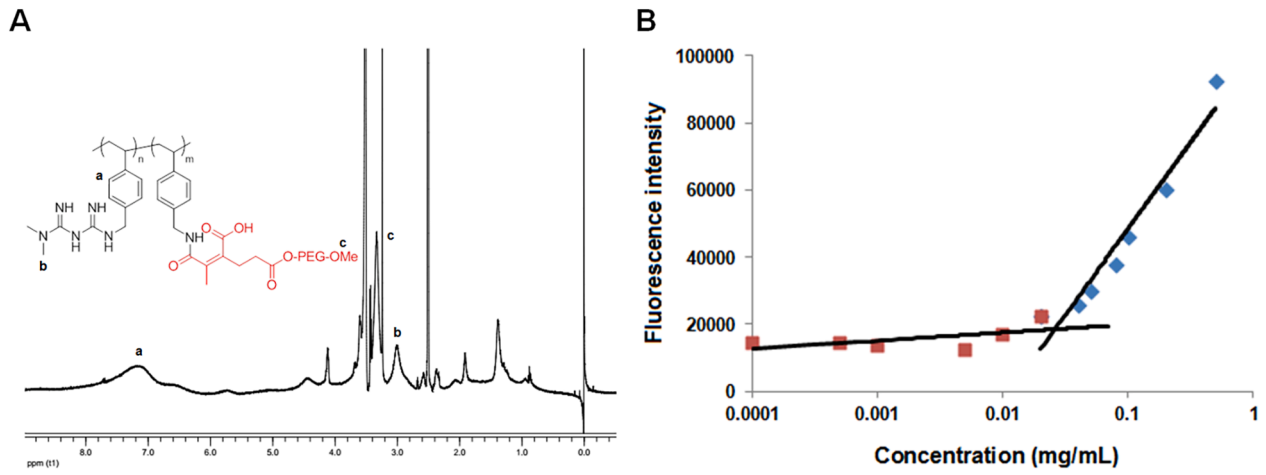

Fig. 1. (A) ^{1}H NMR spectrum of PMet-P(cdmPEG$_{2K}$) polymer in DMSO-d_6; (B) Plots of fluorescence intensity of nile red against PMet-P(cdmPEG$_{2K}$) concentration.

Table 1
Physicochemical characterization of micelles and micelleplexes.

Micelles	Mass ratio (mg: mg)	N/P Ratio	Size (nm)	Zeta potential (mV)	DLC (%)	DLE (%)	Stability (d)
PMet-P(cdmPEG$_{2K}$)	–	–	154	18.2	–	–	–
IL-12 PMet-P(cdmPEG$_{2K}$)	–	20	103	10.3	–	–	10
DOX PMet-P(cdmPEG$_{2K}$)	10:1	–	178	17.1	95.3	9.53	7
	20:1	–	174	14.7	98.2	4.91	7
	30: 1	–	162	16.0	99.9	3.33	8
IL-12/DOX PMet-P(cdmPEG$_{2K}$)	–	20	102	10.4	95.3	9.53	6

vinylbenzylamine **(compound 2)** were synthesized according to protocols in the literature [36,37].

2.2.2. Synthesis of polymetformin (PMet) polymer

4-Vinylbenzyl chloride (1.27 g), **compound 2** (354 mg), AIBN (3 mg), 4-cyano-4-[(dodecylsulfanylthiocarbonyl) sulfanyl] pentanoic acid (24 mg), and 1 mL of dried tetrahydrofuran were added to a Schlenk tube and deoxygenated by free-pump-thawing three times. Then the mixture was filled with N_2 and immersed into an oil bath at 90 °C to start the polymerization. After 24 h, the reaction was quenched by immersing the tube into liquid nitrogen. The mixture was dialyzed against DMSO and then distilled water for 2 days,. The **resulting compound 3** was then lyophilized.

Metformin hydrochloride (1.65 g), **compound 3** (150 mg) and N, N-diisopropylethylamine (1.35 mL) were dissolved in DMSO (4.8 mL) and stirred for 48 h at 110 °C. The reaction mixture was dialyzed against a

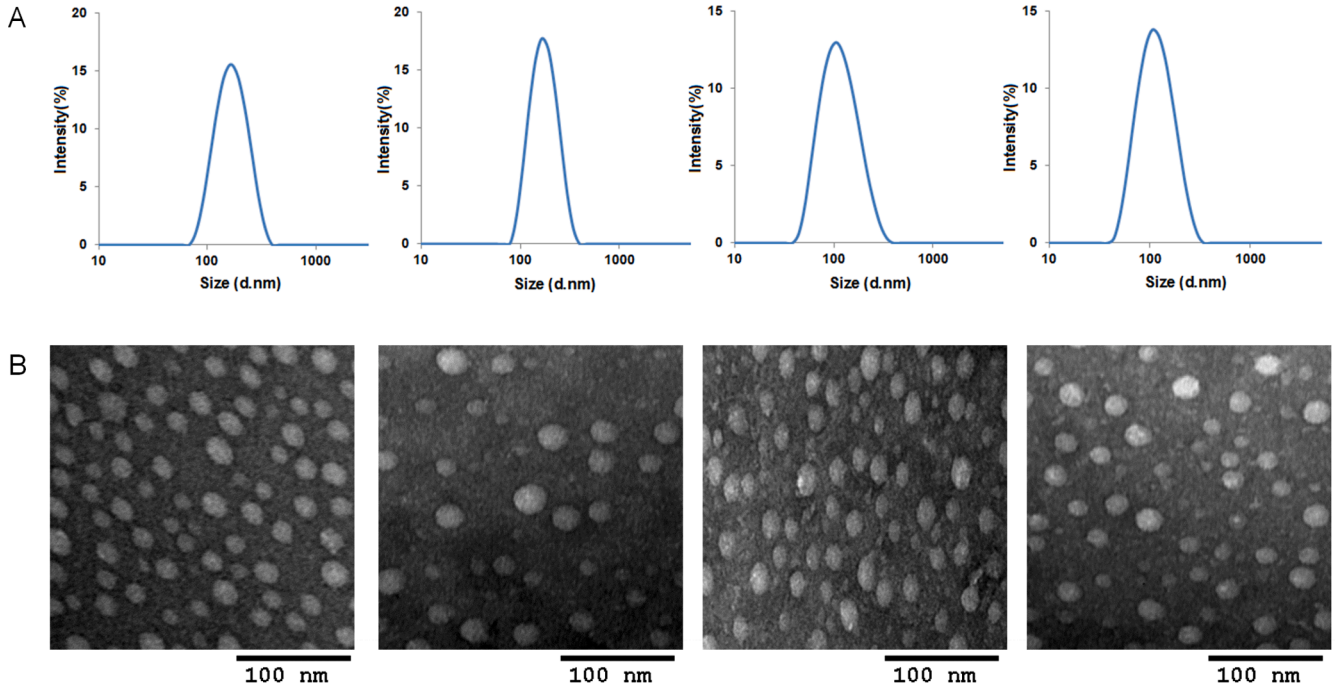

Fig. 2. Particle size distribution (A) and TEM images (B) of blank and DOX-loaded PMet-P(cdmPEG$_{2K}$) micelles, *IL-12* loaded and *IL-12*/DOX co-loaded PMet-P (cdmPEG$_{2K}$) micelleplexes, at the N/P ratio of 20.

0.5% hydrochloride solution in water for 2 days. The Boc-PMet polymer (**compound 4)** was then lyophilized.

The Boc-PMet polymer (**compound 4**) was deprotected at room temperature in DMSO/TFA (1/1, v/v) mixture for 2 h, and then dialyzed against distilled water for 2 days. The Boc-deprotected PMet product with 15% free amino group (**compound 5**) was then lyophilized.

2.2.3. Synthesis of PMet-P(cdmPEG$_{2K}$) polymer

PMet-P(cdmPEG$_{2K}$) was synthesized by a ring opening reaction of PEG$_{2K}$-cdm and pMet polymers. Boc-deprotected PMet (**compound 5**, 100 mg) and PEG$_{2K}$-cdm (**compound 1**, 303 mg) were dissolved in 4 mL of DMSO and stirred at 37 °C for 24 h. The mixture was dialyzed against DMSO and then distilled water for 2 days. The final product of PMet-P (cdmPEG$_{2K}$) polymer was then lyophilized.

^{1}H NMR spectrum was analyzed on a Varian-400 FT-NMR spectrometer at 400 MHz with DMSO-d_6 and $CDCl_3$ as the solvent.

2.3. Preparation and characterization of DOX and pIL-12 co-loaded micelles

2.3.1. Preparation of micelles

Blank and DOX loaded PMet-P(cdmPEG$_{2K}$) micelles were prepared using a thin film hydration method. Briefly, DOX (5 mg/mL in 1:1(v/v) of DCM/methanol) and PMet-P(cdmPEG$_{2K}$) (10 mg/mL in DCM) at designated mass ratios were mixed in a glass tube, and organic solvent was removed through a gentle stream of nitrogen, followed by drying under vacuum for 1 h. The obtained thin-film of PMet-P(cdmPEG$_{2K}$)/DOX mixture was hydrated in HEPES buffer (10 mM, pH 7.4), forming a clear solution of DOX-loaded PMet-P(cdmPEG$_{2K}$) micelles. The blank micelles were prepared as above in the absence of DOX.

For preparation of pIL-12 loaded micelleplexes and pIL-12/DOX co-loaded micelleplexes, equal volumes of pIL-12 and blank micelles or DOX-loaded PMet-P(cdmPEG$_{2K}$) micelles were mixed at various N/P ratios (the ratio of the number of amino groups in PMet-P(cdmPEG$_{2K}$) to the number of phosphate groups in pIL-12), and the mixture was further incubated at room temperature for 20 min.

2.3.2. Gel retardation assay

The pIL-12 binding efficiency of blank and DOX loaded PMet-P (cdmPEG$_{2K}$) micelles was analyzed by agarose gel electrophoresis. The pIL-12 loaded PMet-P(cdmPEG$_{2K}$) micelleplexes and pIL-12/DOX co-loaded PMet-P(cdmPEG$_{2K}$) micelleplexes, containing 0.5 μg of pIL-12 prepared at various N/P ratios from 1 to 20, and DOX loaded micelles with equal DOX concentrations as in the counterparts of pIL-12/DOX co-loadeded micelleplexes, were loaded onto a 0.8% agarose gel and run under tris–acetate (TAE) buffer at 80 V for 45 min. pIL-12 retardation was visualized and photographed using a ChemiDoc XRS imaging system (Bio-Rad, Hercules, CA, USA).

2.3.3. Characterizations of micelles and micelleplexes

The size distribution and zeta potential of blank and DOX-loaded micelles, and pIL-12 loaded and pIL-12/DOX co-loaded micelleplexes at various N/P ratios, were examined by dynamic light scattering (DLS) through a Malvern Zeta Nanosizer. The morphology was observed by transmission electron microscopy (TEM) using a negative staining method.

The critical micellar concentration (CMC) of PMet-P(cdmPEG$_{2K}$) was measured by fluorescence intensity using nile red as a probe. Briefly, nile red and differing amounts of PMet-P(cdmPEG$_{2K}$) dissolved in DCM were put into tubes, the solvent was removed by nitrogen flow and the formed thin film was dried under vacuum. HEPES was added to yield a final nile red concentration of 6.0×10^{-7} M, with the PMet-P(cdmPEG$_{2K}$) micelle concentrations ranging from 1.0×10^{-4} to 5×10^{-1} mg/mL. Fluorescence was carried out with excitation at 550 nm and emission spectra recorded from 570 to 720 nm. The CMC value was determined as the cross-point when extrapolating the intensity at low and high concentration regions.

The DOX concentration was assayed by high performance liquid chromatography (HPLC), detected by a Waters 2475 Fluorescence Detector with excitation at 490 nm and emission at 590 nm. The drug encapsulation efficiency (DEE) and drug loading capacity (DLC) were calculated by the following equations (1–2).

$$DEE(\%) = \frac{W_{PTX\ incorported\ in\ micelle}}{W_{Total\ PTX\ added\ in\ micelle}} \times 100 \quad (1)$$

$$DLC(\%) = \frac{W_{PTX\ incorported\ in\ micelle}}{W_{Total\ \ micelle}} \times 100 \quad (2)$$

The serum stability of the PMet-P(cdmPEG$_{2K}$) micelles co-loaded with pIL-12 and DOX was studied to evaluate the shielding effect of PEG in preventing aggregation in serum. The pIL-12/PEI$_{25K}$ polyplexes, blank PMet-P(cdmPEG$_{2K}$) micelles, pIL-12, DOX and pIL-12/DOX loaded micelles, were mixed with a BSA solution (1 mg/mL) in HEPES buffer (10 mM, pH 7.4) under gentle stirring. The average sizes of micelles were monitored over time by a Malvern Zeta Nanosizer.

2.3.4. Tumor extracellular pH (pHe) sensitivity

The sensitivity of pIL-12/DOX co-loaded PMet-P(cdmPEG$_{2K}$) micelleplexes to the acidic pH was evaluated by examining changes in the zeta potentials at different pHs. The pIL-12 loaded and pIL-12/DOX co-loaded PMet-P(cdmPEG$_{2K}$) micelleplexes were incubated in HEPES (10 mM) buffer at pH 7.4 and pH 6.8 at 37 °C. Aliquots of the micelleplex solutions were withdrawn at designated time intervals and the zeta potential was measured with a Malvern Zeta Nanosizer.

2.3.5. In vitro drug release

In vitro DOX release profile was investigated by the dynamic dialysis method. Typically, DOX loaded micelles and pIL-12/DOX co-loaded PMet-P(cdmPEG$_{2K}$) micelleplexes with 0.5 mg of DOX were transferred into a dialysis bag (molecular weight cutoff = 3500) and immersed in 80 mL of HEPES (10 mM) buffer at pH 7.4 or pH 6.8, while stirring at 100 rpm and a temperature of 37 °C. DOX release from DOX loaded micelles and pIL-12/DOX co-loaded PMet-P(cdmPEG$_{2K}$) micelleplexes was assayed at predetermined times by fluorescence spectrometry with excitation at 490 nm and emission at 590 nm. The DOX diffusion profile from the DOX solution was also investigated for comparison.

2.4. Cell culture

4T1.2 is a mouse metastatic breast cancer cell line, which was cultured in DMEM culture medium, containing 10% (v/v) fetal bovine serum and 100 IU/mL penicillin and 100 μg/mL streptomycin at 37 °C in a humidified 5% CO_2-95% air atmosphere.

2.5. In vitro cytotoxicity

2.5.1. In vitro cytotoxicity of micelleplexes

In vitro cytotoxicity of PMet-P(cdmPEG$_{2K}$) micelleplexes with pEGFP was measured using the MTT method with PEI$_{25K}$ and pEGFP/PEI$_{25K}$ polyplexes as controls. 4T1.2 cells were seeded onto a 96-well plate at a density of 3×10^3 cells/well and incubated for 24 h. Culture were treated with PEI$_{25K}$, pEGFP/PEI$_{25K}$ polyplex, PMet-P(cdmPEG$_{2K}$) micelles and pEGFP/PMet-P(cdmPEG$_{2K}$) micelleplexes of various N/P ratios in FBS-free culture medium (Life Technologies, USA) at pH 7.4 and pH 6.8 for 4 h. The culture medium was then replaced with fresh complete medium at pH 7.4. After further incubation for 44 h, the MTT assay was carried out as previously described [35,38]. Relative cell viability was calculated by the following Eq. (3):

$$Cell\ viability(\%) = \frac{A_{sample} - A_{blank}}{A_{control} - A_{blank}} \times 100 \quad (3)$$

A_{sample} and $A_{control}$ are the absorbance in the presence and absence of

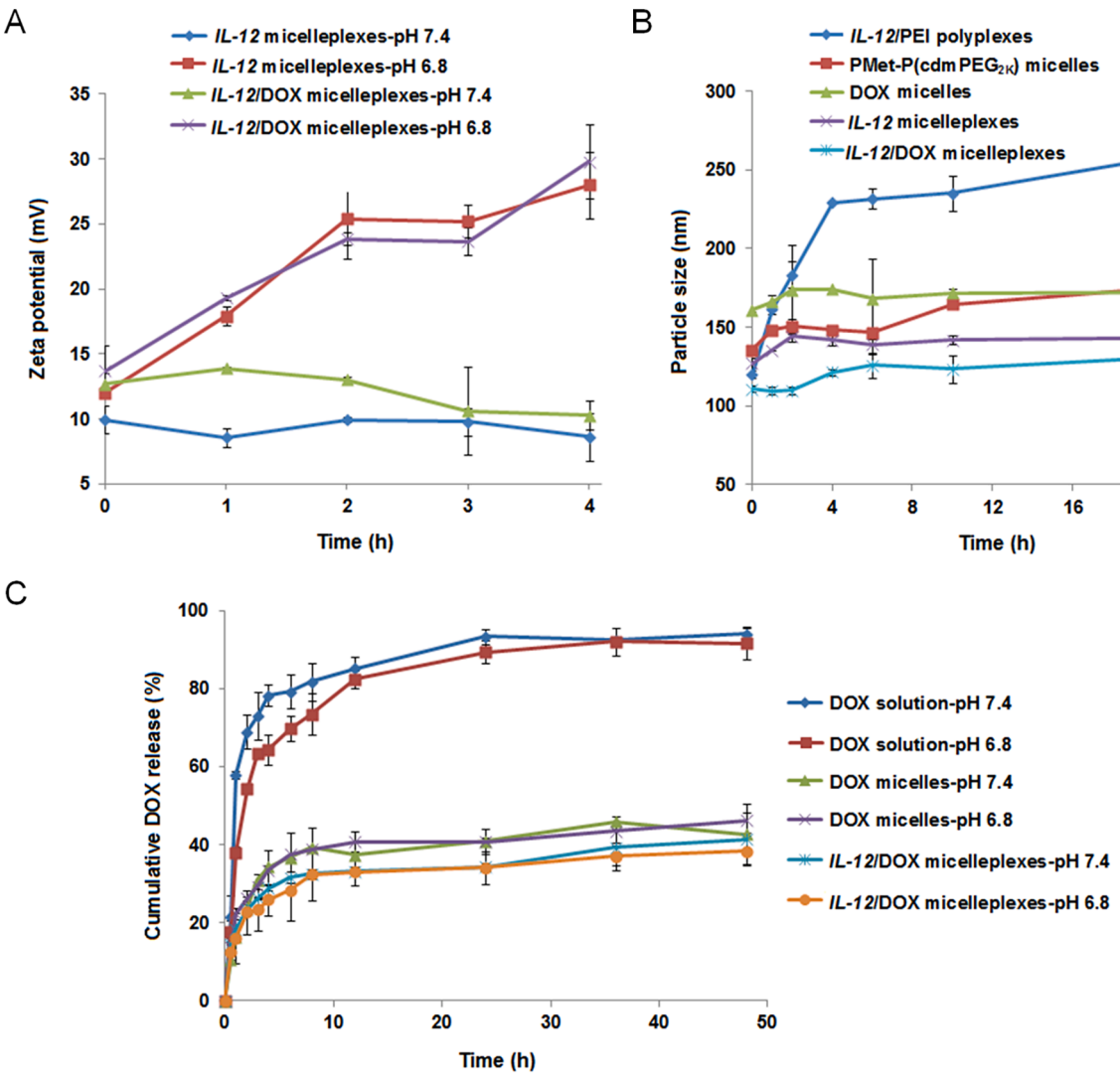

Fig. 3. (A) Zeta potential changes of *IL-12* PMet-P(cdmPEG$_{2K}$) micelleplexes and *IL-12*/DOX PMet-P(cdmPEG$_{2K}$) micelleplexes incubated at pH 7.4 and pH 6.8 in Hepes buffer. (B) Particle size changes in *IL-12*/PEI$_{25K}$ polyplexes, blank and DOX-loaded PMet-P(cdmPEG$_{2K}$) micelles, *IL-12* and *IL-12*/DOX PMet-P(cdmPEG$_{2K}$) micelleplexes as a function of incubation time with 1 mg/mL BSA solution at pH 7.4. (C) Cumulative DOX release profiles of DOX-loaded and *IL-12*/DOX co-loaded PMet-P(cdmPEG$_{2K}$) micelleplexes into the medium at pH 7.4 and pH 6.8 with DOX as the control.

sample treatment, respectively. A_{blank} is the absorbance of culture medium.

2.5.2. *In vitro cytotoxicity of DOX-loaded formulations*

4T1.2 cells were seeded onto a 96-well plate at a density of 3×10^3 cells/well and incubated for 24 h. DOX solution, blank, and DOX-loaded PMet-P(cdmPEG$_{2K}$) micelles, pIL-12 loaded, or pIL-12/DOX co-loaded micelleplexes, were placed into culture medium at different concentrations and at pH 7.4 or pH 6.8, and then were added to the cells and incubated for 72 h. MTT assays were carried out as previously described. The relative cell viability was calculated by the equation provided above.

2.6. *Cellular uptake and intracellular trafficking*

4T1.2 cells were seeded onto glass-bottom dishes (In Vitro Scientific, USA) at a density of 1×10^5 cells/dish. Following incubation for 24 h, cells were treated with DOX solution, DOX loaded micelles, or pIL-12/DOX co-loaded PMet-P(cdmPEG$_{2K}$) micelleplexes in FBS-free culture medium (Life Technologies, USA) at pH 7.4 or pH 6.8 for 4 h. The concentration of DOX was kept at 20 μg/mL. Cells were then stained with Hoechst 33,342 (1 mg/mL) for 20 min, and LysoTracker Green DND-26 (50 nM, Invitrogen, USA) for 30 min, followed by washing with cold PBS. The intracellular distribution of DOX formulations was observed under a CLSM. Fluorescence intensity was quantified using Image J based on 3 different areas and 50–100 cells.

2.7. *In vitro gene transfection efficiency*

In vitro gene transfection efficiency of pLuc loaded PMet-P(cdmPEG$_{2K}$) micelleplexes was evaluated using 4T1.2 cells. 4T1.2 cells were seeded onto a 96-well plate at a density of 3×10^4 cells/well and incubated for 24 h. The cells were incubated with PEI$_{25K}$ polyplexes and PMet-P(cdmPEG$_{2K}$) micelleplexes at different N/P ratios in FBS-free culture medium at pH 7.4 or 6.8 for 4 h. The culture medium was then replaced with fresh complete medium at pH 7.4. After further incubation for 44 h, the cells were washed with PBS and lysed with luciferase cell culture lysis buffer. The lysates were transferred to a 96-well plate, assay buffer was added and the luciferase activity was measured using a microplate reader (Model 550, Bio-Red, USA). The protein content of the lysed cells was determined using a BCA Protein Assay kit (Invitrogen, USA). The transfection efficiency of luciferase

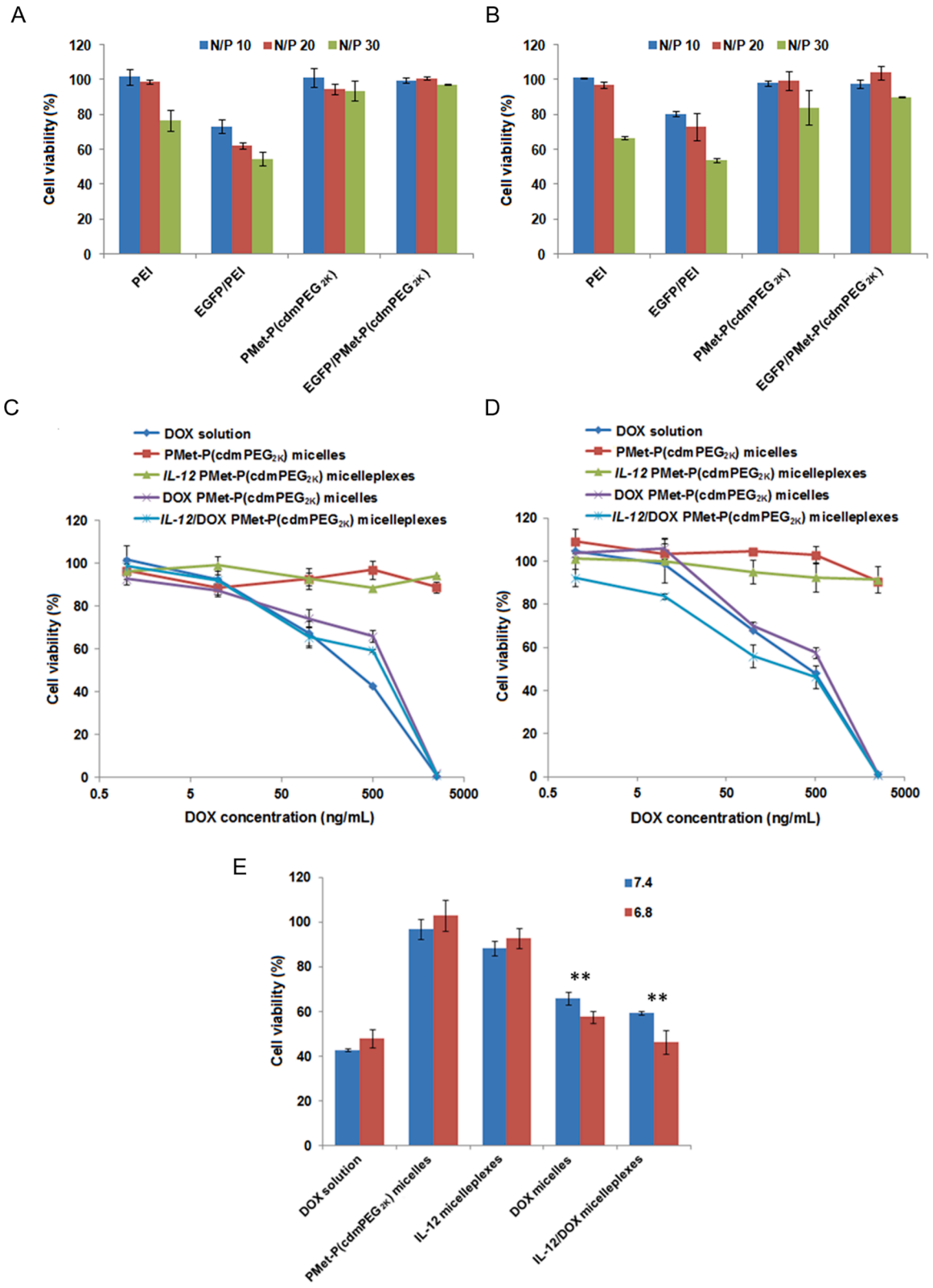

Fig. 4. In vitro cytotoxicity of PEI_{25K} and EGFP/PEI_{25K} polyplexes, PMet-P(cdmPEG$_{2K}$) micelles and EGFP/PMet-P(cdmPEG$_{2K}$) micelleplexes at various N/P ratios against 4T1.2 cells after 4 h incubation in FBS-free culture medium at pH 7.4 (A) and pH 6.8 (B) and after 48 h incubation in culture medium (pH 7.4) containing 10% FBS. In vitro cell viability profiles of DOX solution, PMet-P(cdmPEG$_{2K}$) micelles, DOX-loaded PMet-P(cdmPEG$_{2K}$) micelles, *IL-12* loaded and *IL-12*/DOX co-loaded PMet-P(cdmPEG$_{2K}$) micelleplexes against 4T1.2 cells after 72 h incubation in culture medium at pH 7.4 (C) and pH 6.8 (D). (E) In vitro cytotoxicity of DOX solution, PMet-P(cdmPEG$_{2K}$) micelles, DOX-loaded PMet-P(cdmPEG$_{2K}$) micelles, *IL-12* loaded and *IL-12*/DOX co-loaded PMet-P(cdmPEG$_{2K}$) micelleplexes against 4T1.2 cells after 72 h incubation in culture medium at pH 7.4 and pH 6.8 at a DOX concentration of 500 ng/mL.

Table 2
IC_{50} values of DOX solution, DOX-loaded micelles and *IL-12*/DOX co-loaded PMet-P($cdmPEG_{2K}$) micelleplexes against 4T1.2 cells after 72 h of incubation in culture medium at pH 7.4 and pH 6.8.

Micellar formulations	IC_{50} at pH 7.4 (μg/mL)	IC_{50} at pH 6.8 (μg/mL)
DOX solution	0.381	0.443
DOX micelles	0.998	0.768
IL-12/DOX micelleplexes	0.819	0.348

pDNA was expressed as relative light units per mg protein (RLU/mg protein).

The in vitro Cy3-siRNA transfection efficiency was quantified by flow cytometry. 4T1.2 cells were seeded onto a 96-well plate at a density of 3×10^4 cells/well. Following incubation for 24 h, cells were treated with free Cy3-labeled siRNA, Cy3-labeled siRNA/PEI_{25K} complex, or Cy3-labeled siRNA loaded PMet-P($cdmPEG_{2K}$) micelleplexes in FBS-free culture medium (Life Technologies, USA) at pH 7.4 or pH 6.8 for 4 h, respectively. The concentration of Cy3-labeled siRNA was kept at 10 pmol. The transfected cells were harvested, resuspended in PBS, and then analyzed by LSRFortessa (BD Biosciences). The data were analyzed with the FlowJo software (Tree Star Inc.) and reported as mean fluorescence intensity.

2.8. DOX and FAM-siRNA co-delivery via the micellar system

4T1.2 cells were seeded onto a 96-well plate (In Vitro Scientific, USA) at a density of 2×10^4 cells/well. Following incubation for 24 h, cells were treated with free FAM-labeled siRNA, DOX-loaded micelles, FAM-siRNA loaded, or FAM-siRNA/DOX co-loaded PMet-P($cdmPEG_{2K}$) micelleplexes in FBS-free culture medium (Life Technologies, USA) at pH 7.4 and 6.8 for 4 h, respectively. The concentrations of DOX and FAM-labeled siRNA were kept at 5 μg/mL and 10 pmol, respectively. Then cells were stained with 1 mg/mL of Hoechst 33,342 (Invitrogen, USA) for 20 min, followed by washing with ice-cold PBS. The intracellular distribution of DOX and FAM-siRNA was observed under a confocal laser scanning microscope (CLSM, FluoView 1000, Olympus, Japan).

2.9. Animals

Female BALB/c mice (6–8 weeks old) were purchased from Charles River Laboratories (Davis, CA) and housed under AAALAC guidelines. The mouse experiments were approved by the Institutional Animal Care and Use Committee at the University of Pittsburgh and carried out according to institutional guidelines.

2.10. In vivo gene transfection efficiency

pEGFP was used as a reporter gene to evaluate the plasmid transfection efficiency of micelleplexes in vivo. Female BALB/c mice were inoculated subcutaneously with 4T1.2 cells (4×10^5 cells/mouse). When the tumor size reached approximately 500 mm^3, 200 μL of pEGFP/PEI_{25K} polyplexes and pEGFP loaded PMet-P($cdmPEG_{2K}$) micelleplexes in 5% dextrose solution were intravenously injected by tail vein at an pEGFP dose of 50 μg/mouse. After 23 h, 200 μL of Hoechst 33342 (5 mg/kg in PBS) was intravenously injected to stain the nuclei of cells. One hour later, the mice were killed, tissues were excised, frozen, and sectioned into 25 μm slices with a cryostat. The slices were mounted and observed by CLSM. The mice only treated with Hoechest 33342 were included as a negative control. Fluorescence intensity was quantified using Image J based on 3 different areas and 50–100 cells.

AF647-labeled siRNA was utilized to evaluate the siRNA transfection efficiency of micelleplexes in vivo. Mice were inoculated with tumor cells as described above. When the tumor size reached approximately 500 mm^3, 200 μL of AF647-siRNA/PEI_{25K} polyplexes and AF647-siRNA loaded PMet-P($cdmPEG_{2K}$) micelleplexes in 5% dextrose solution were injected intravenously by tail vein at an AF647-siRNA dose of 3 nmol/mouse. Two hundred μL of Hoechst 33342 (5 mg/kg in PBS) was intravenously injected to stain the nuclei of cells after 5, 15 or 23 h. One hour later, the mice were sacrificed and the tissues were excised. 25 μm frozen sections were prepared. The slices were mounted and observed under a CLSM.

2.11. In vivo therapeutic efficacy

4T1.2 cells were inoculated into female BALB/c mice 2×10^5 cells per mouse. When the tumor grew to ~50 mm^3, mice were injected intravenously with saline, DOX-loaded PMet-P($cdmPEG_{2K}$) micelles, pIL-12 loaded and pIL-12/DOX co-loaded PMet-P($cdmPEG_{2K}$) micelleplexes at a DOX dose of 5 mg/kg and an pIL-12 dose of 50 μg/mouse, on days 0, 5, 10 and 15. Tumor volumes were calculated by the formula: $(L \times W^2)/2$, in which L is the longest and W is the shortest tumor diameter (mm). Body weights were monitored during the entire experiment. Tumor tissues were collected, fixed in 10% formaldehyde, and embedded in paraffin. After sectioning into 5 μm slices, sections were stained with hematoxylin and eosin (H&E) and examined using a Zeiss Axiostar plus Microscope (PA, USA).

2.12. Statistical analysis

Statistical analysis was performed using two-tailed Student's *t* test when comparing two groups, and one-way analysis of variance (ANOVA) when comparing more than 2 groups, followed by a Newman-Keuls test if the overall ANOVA was statistically significant ($p < 0.05$). In all statistical analyses, $p < 0.05$ was defined as statistically significant.

3. Results

3.1. Synthesis and characterization of PMet-P($cdmPEG_{2K}$) polymer

The synthesis route of the PMet-P($cdmPEG_{2K}$) polymer is shown in Scheme 1. Firstly, PEG_{2K}-cdm (**compound 1**) and Boc-protected 4-vinylbenzylamine monomer **(compound 2)** were synthesized according to prior literature [39]. **Compound 3** was synthesized by reversible addition fragment chain transfer (RAFT) polymerization of 4-vinylbenzyl chloride and **compound 2.** NMR confirmed that **Compound 3** consisted of 85% of 4-vinylbenzyl chloride and 15% of Boc-protected 4-vinylbenzylamine moieties. In the next step, MET was conjugated to **compound 3** to obtain **compound 4**. The Boc-groups of the **compound 4** were deprotected to yield amine-bearing **compound 5,** which was further conjugated with PEG_{2K}-cdm to generate PMet-P(cdmPEG2K) polymer.

The chemical structure of the PMet-P($cdmPEG_{2K}$) polymer was confirmed by ^1H NMR, as shown in Fig. 1**A**. The peaks at 6.0–8.0 ppm showed the ethylene protons (a, —CH═CH—) of the benzene ring located in the polystyrene backbone. The characteristic peaks appearing at 3.1 ppm represent the protons (c, —OCH_3) of the PEG_{2K} chain. The peak at 2.9 ppm is attributed to the methyl protons of MET (b, N-CH3). These peaks suggest the successful synthesis of the PMet-P($cdmPEG_{2K}$) polymer.

The unit number of MET per PMet-P($cdmPEG_{2K}$) molecule was calculated to be 42 by the relative intensity ratio of the methyl protons (b, N-CH_3) of MET to the ethylene protons (a, —CH═CH—) of the benzene ring. The unit number of PEG_{2K} chain conjugated to the PMet-P ($cdmPEG_{2K}$) molecule was calculated to be 12 by the relative intensity ratio of the protons (c, —OCH_3) of the PEG_{2K} chain to the ethylene protons (a, —CH═CH—) of the benzene ring.

In addition, the CMC value of the PMet-P(cdmPEG2K) was measured at 28.6 μg/mL (Fig. 1B).

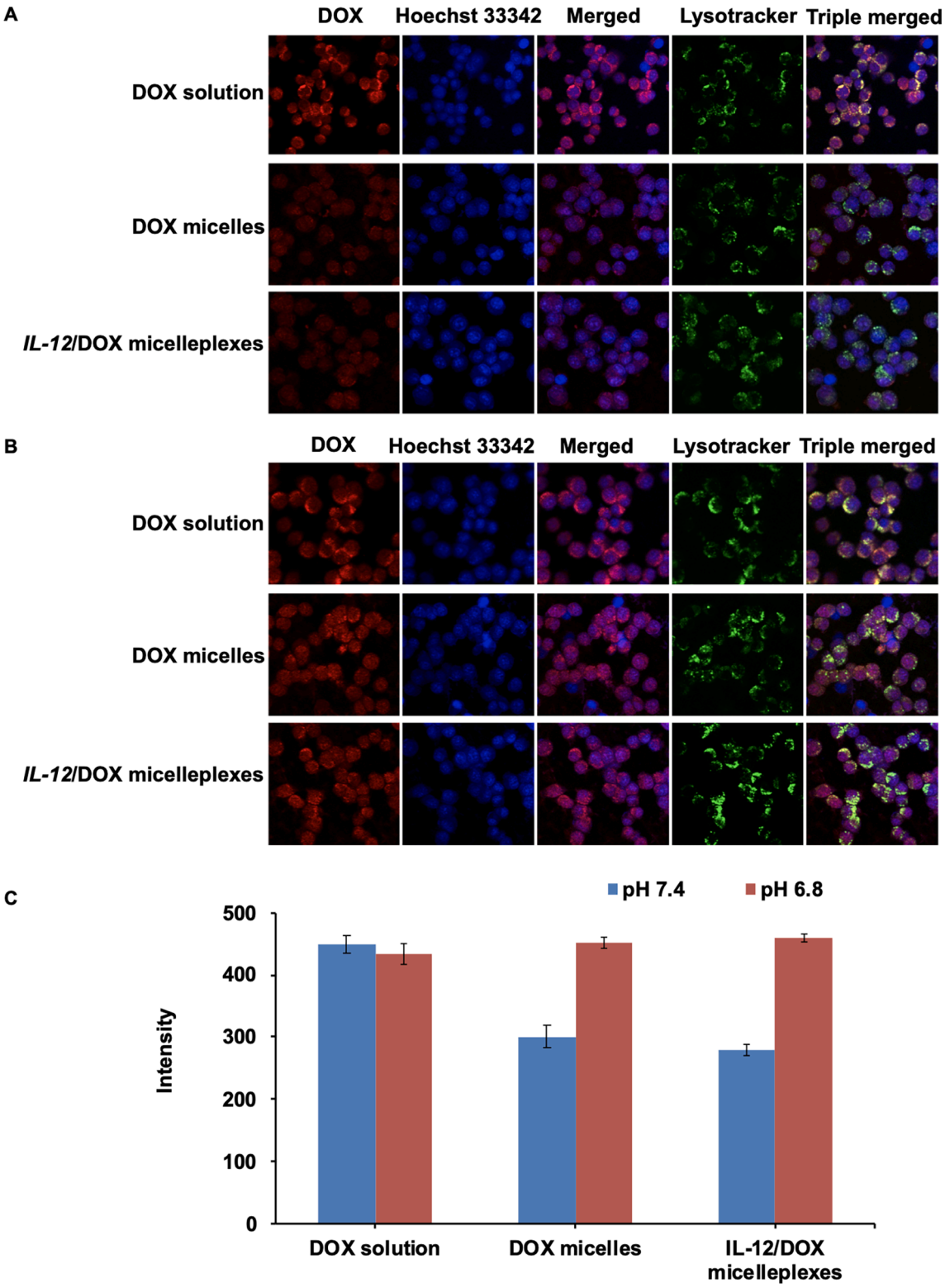

Fig. 5. CLSM of 4T1.2 cells after incubation with DOX.HCl solution, DOX-loaded PMet-P(cdmPEG$_{2K}$) micelles and *IL-12*/DOX co-loaded PMet-P(cdmPEG$_{2K}$) micelleplexes for 4 h in FBS-free culture medium at pH 7.4 (A) and pH 6.8 (B). (C) Quantification of the DOX fluorescence intensity by Image J.

3.2. Preparation and characterization of the micelles and micelleplexes

DOX loaded PMet-P(cdmPEG$_{2K}$) micelles were prepared using the thin film hydration method and the DOX/PMet-P(cdmPEG$_{2K}$) micelles were further complexed with pIL-12 through electrostatic interaction to yield the DOX/pIL-12 co-loaded micelleplexes. Gel retardation assays confirmed the formation of micelleplexes with or without co-loaded DOX at an NP ratio of 5 and above (data not shown). The DNA-condensing capacity of the PMet-P(cdmPEG$_{2K}$) micelles was further examined by dynamic light scattering. Blank micelles and the DOX/PMet-P(cdmPEG$_{2K}$) micelles showed an average size of 154 nm and 178 nm respectively (Table 1 and Fig. 2A). Moreover, they were able to

efficiently condense pIL-12 into a more compact micelleplex structure with a smaller particle size of 103 and 102 nm at an N/P ratio of 20. This is the ratio at which all subsequent in vivo studies (gene transfection and therapeutic efficacy) were conducted. In addition, after complexation with pIL-12, the zeta potentials of blank and DOX-loaded micelles decreased from 18.2 and 17.1 mV to 10.3 and 10.4 mV. The micelles and micelleplexes observed by TEM showed compact and spherical morphology (Fig. 2B). In addition, the PMet-P(cdmPEG$_{2K}$) micelles were effective in loading DOX, with a DLC and DLE of 9.53% and 99.9% (Table 1).

To demonstrate that the PEG shell could be detached from the PMet-P(cdmPEG$_{2K}$) micelleplexes at lower pH, the pH sensitivity of pIL-12 loaded and pIL-12/DOX co-loaded micelleplexes was investigated by monitoring the changes in zeta potentials at pH 7.4 and pH 6.8 over time. As shown in Fig. 3A, the surface charge of micelleplexes increased significantly from 10.7 mV to 29.8 mV after 4 h incubation at pH 6.8. In comparison, the zeta potential of micelleplexes showed no significant change over the same period of time at pH 7.4.

The serum stability of micelles and micelleplexes was investigated through monitoring the size changes at different time intervals after co-incubation with bovine serum albumin (BSA, 1 mg/mL) (Fig. 3B). "Gold-standard" transfection agent PEI$_{25K}$ complexed with pIL-12 was included as a control. PMet-P(cdmPEG$_{2K}$) micelles and micelleplexes only showed slight increases in size after 24 h incubation, but pIL-12/PEI$_{25K}$ polyplexes quickly formed significantly larger aggregates. These results suggest that the positive charge-shielding effect of PEG on the PMet-P(cdmPEG$_{2K}$) micellar surface can enhance the serum stability of micelles and micelleplexes after intravenous injection.

3.3. In vitro drug release

The release pattern of DOX from DOX-loaded micelles and pIL-12/DOX co-loaded PMet-P(cdmPEG$_{2K}$) micelleplexes was studied using a dynamic dialysis method at pH 7.4 and pH 6.8. DOX solution was included for comparison. As shown in Fig. 3C, almost all DOX was diffused from the dialysis bag after 12 h at pH 7.4 or pH 6.8. DOX loaded into PMet-P(cdmPEG$_{2K}$) micelles and micelleplexes showed a sustained release over 48 h under both physiological pH (pH 7.4) and more acidic pH (pH 6.8). In addition, the DOX release from micelleplexes was much slower than that from micelles. There were no significant differences in the DOX release from micelles and micelleplexes at pH 7.4 vs. pH 6.8.

3.4. In vitro cytotoxicity

Biocompatibility is a critical parameter for a drug and gene delivery system. In this study, the cytotoxicity of the PMet-P(cdmPEG$_{2K}$) micelles and the pEGFP/PMet-P(cdmPEG$_{2K}$) micelleplexes was evaluated using PEI$_{25K}$ and pEGFP/PEI$_{25K}$ polyplexes as controls. It is well known that the PEI$_{25K}$ polymer, particularly its complexes with DNA, shows a high level of nonspecific cytotoxicity. Similar results were observed in our study at both pH 7.4 (Fig. 4A) and pH 6.8 (Fig. 4B). The levels of cytotoxicity of PEI$_{25K}$ and pEGFP/PEI$_{25K}$ were significantly increased with an increase in the N/P ratio to 30; however, no obvious inhibition of cell proliferation was detected using the PMet-P(cdmPEG$_{2K}$) micelles or the pEGFP/PMet-P(cdmPEG$_{2K}$) micelleplexes at pH 7.4 and pH 6.8, even at an N/P ratio of 30. These data indicate that the PMet-P(cdmPEG$_{2K}$) carrier and the pEGFP/PMet-P(cdmPEG$_{2K}$) micelleplexes are biocompatible and nontoxic and may be used as a safe nanocarrier for co-delivery of anticancer agents and genes.

The cytotoxicity of DOX-loaded micelles and pIL-12/DOX co-loaded micelleplexes was examined using an MTT assay in 4T1.2 cells at pH 7.4 (Fig. 4C) and pH 6.8 (Fig. 4D). Compared with DOX-loaded micelles and pIL-12/DOX co-loaded micelleplexes, the DOX solution alone showed stronger cytotoxicity at a DOX concentration of 500 ng/mL, due to rapid uptake via passive diffusion (Fig. 4E). Additionally, pIL-12/DOX co-loaded micelleplexes were more effective than DOX-loaded micelles. More importantly, DOX-loaded micelles and pIL-12/DOX co-loaded PMet-P(cdmPEG$_{2K}$) micelleplexes displayed a pH-dependent cytotoxicity, and showed much improved inhibition of cell proliferation at pH 6.8. The calculated IC$_{50}$ (half maximal inhibitory concentration) for DOX-loaded formulations at the two pHs are summarized in Table 2. Free DOX showed comparable cytotoxicity at the two pHs with an IC50 of 0.381 μg/mL (pH 7.4) and 0.441 μg/mL (pH 6.8). The IC$_{50s}$ of DOX-loaded and pIL-12/DOX co-loaded PMet-P(cdmPEG$_{2K}$) micelleplexes were 0.768 μg/mL and 0.348 μg/mL at pH 6.8, which were significantly lower than the corresponding values at pH 7.4 (0.998 and 0.819 μg/mL). These results suggest that incorporation of pIL-12 into DOX-loaded PMet-P(cdmPEG$_{2K}$) provides improved cytotoxicity, in addition to potential synergy between IL and 12 and DOX in vivo.

3.5. Cellular uptake and intracellular trafficking

Intracellular uptake and distribution of DOX-loaded micelles and pIL-12/DOX co-loaded PMet-P(cdmPEG$_{2K}$) micelleplexes were investigated by CLSM (Fig. 5). After 4 h incubation, much stronger intracellular fluorescence was observed for both DOX loaded micelles and pIL-12/DOX co-loaded micelleplexes at pH 6.8 compared to pH 7.4, and DOX fluorescence was mainly localized in the nuclei. In contrast, cellular uptake of free DOX was not significantly affected by pH, which showed slightly stronger fluorescence compared with DOX loaded micellar formulations, due to the rapid passive diffusion of free DOX. In addition, compared to DOX-loaded micelles, pIL-12/DOX co-loaded PMet-P(cdmPEG$_{2K}$) micelleplexes exhibited increased cellular uptake. These data are consistent with the cytotoxicity results, further confirming that the PEG de-shielding property of the PMet-P(cdmPEG$_{2K}$) micelleplexes at the lower pH led to the increased intracellular co-delivery of DOX and pIL-12, and thus enhanced inhibition of tumor cell proliferation.

3.6. In vitro gene transfection efficiency

To evaluate the potential application of the PMet-P(cdmPEG$_{2K}$) micelles for gene delivery, in vitro gene transfection efficiency was evaluated in 4T1.2 cells by using luciferase reporter genes (pLuc) (Fig. 6). pDNA/PEI$_{25K}$ polyplexes were used as a positive control. pLuc/PEI$_{25K}$ polyplexes showed the highest level of luciferase expression at a N/P ratio of 20. The luciferase expression of pLuc/PMet-P(cdmPEG$_{2K}$) micelleplexes was greatly enhanced with the increase of N/P ratio and reached the peak level at a N/P ratio of 20. Further increases in the N/P

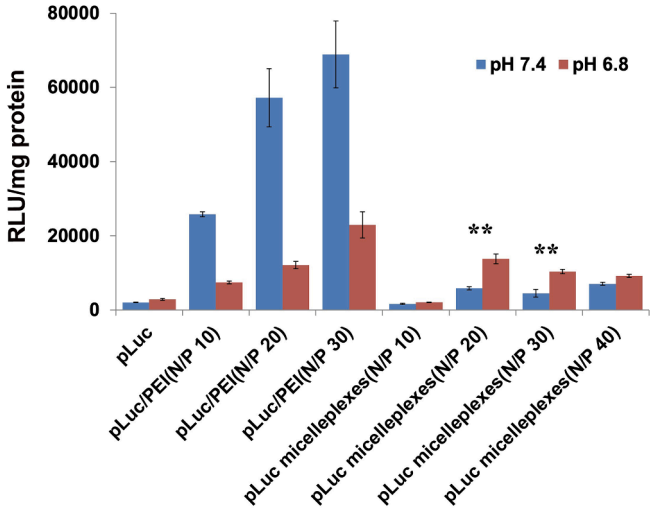

Fig. 6. Luciferase expression determined of pLuc/PEI$_{25K}$ and pLuc/PMet-P(cdmPEG$_{2K}$) micelleplexes at different N/P ratios. The treated cells were incubated in FBS-free culture medium at pH 7.4 and pH 6.8 for 4 h and further incubated in culture medium at pH 7.4 containing 10% FBS for 48 h.

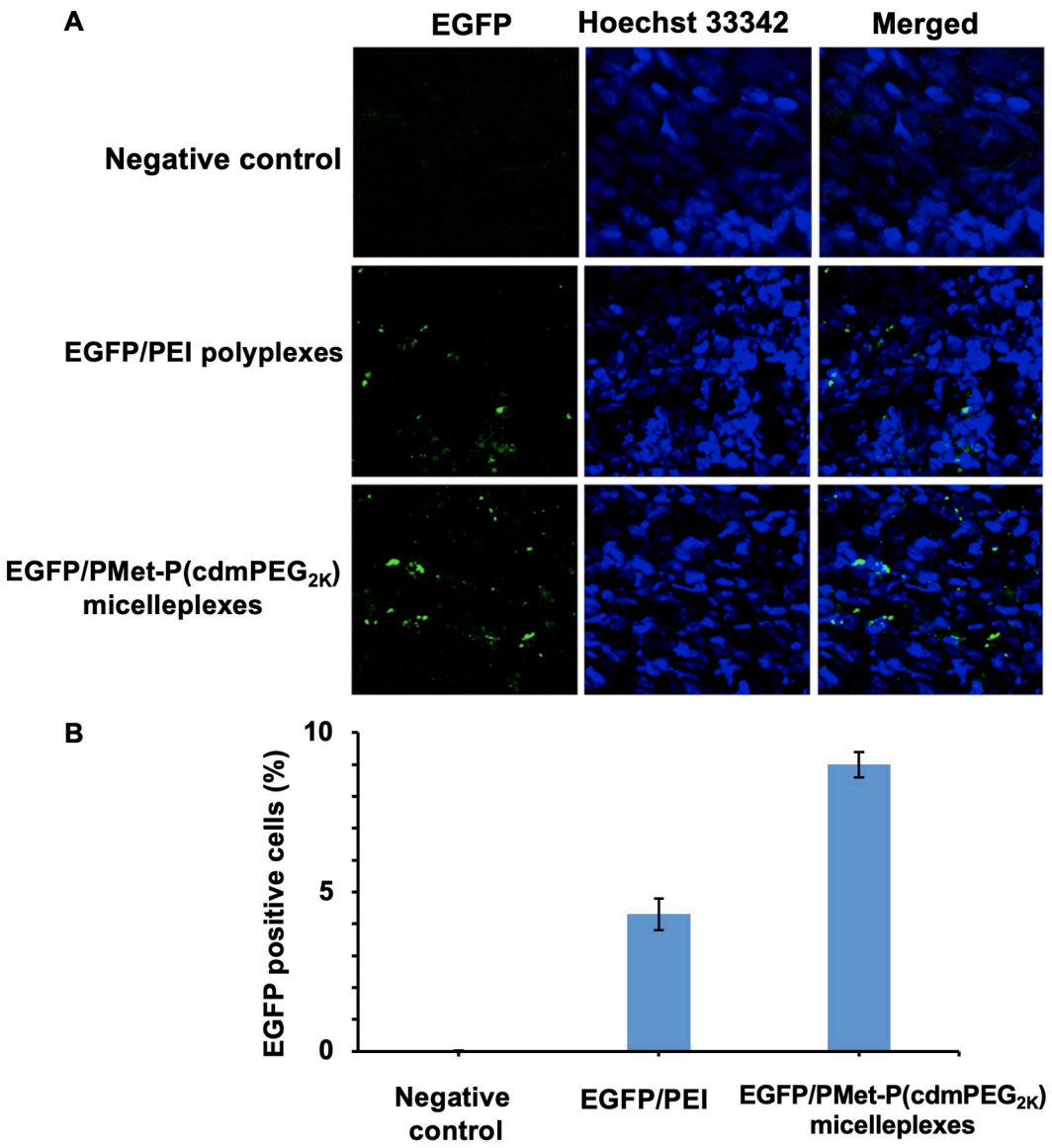

Fig. 7. (A) Cryo-section of EGFP expression in tumor observed under CLSM after treatment with negative control, EGFP/PEI_{25K} polyplexes and EGFP/PMet-P ($cdmPEG_{2K}$) micelleplexes for 24 h in 4T1.2 tumor-bearing mice (EGFP dose: 25 μg/mice). Negative control represents mice treated only with Hoechst 33342. (B) Quantification of the percentage of GFP positive cells by Image J.

ratio resulted in decreased transfection for pLuc/PMet-P($cdmPEG_{2K}$) micelleplexes. PEI_{25K} was more effective in transfection at pH 7.4 - luciferase expression was approximately 10-fold higher than that achieved with the PMet-P($cdmPEG_{2K}$) micelles. The level of transgene expression from pLuc/PEI polyplexes dropped significantly at pH 6.8. In contrast, increased transfection was detected for pLuc/PMet-P ($cdmPEG_{2K}$) micelleplexes at pH 6.8, compared to that at pH 7.4, suggesting that de-shielding of the PEG layer of PMet-P(cdmPEG2K) micelles under the more acidic tumor microenvironment led to more pDNA being delivered into the tumor cells, and subsequently increased transgene expression.

3.7. *In vivo gene transfection efficiency*

After demonstrating the de-shielding of PMet-P($cdmPEG_{2K}$) in response to pH, and the effective co-delivery of DOX and pIL12 to tumor cells in vitro, the efficiency of this carrier in delivering a transgene to tumors was further evaluated in 4T1.2 tumor-bearing mice. A N/P ratio of 20 was used based on the results of in vitro biophysical and biological evaluations. Transgene expression was examined in tumors 24 h following intravenous injection of PEI_{25K} and PMet-P($cdmPEG_{2K}$) micelles carrying pEGFP (Fig. 7). Low levels of EGFP were observed in 4T1.2 tumors of mice treated with pEGFP/PEI_{25K} polyplexes. In comparison, higher levels of EGFP were detected in tumors from mice treated with EGFP/PMet-P($cdmPEG_{2K}$) micelleplexes (Fig. 7**A**). In addition, more GFP-positive cells were observed with pEGFP/ PMet-P ($cdmPEG_{2K}$) treatment compared to pEGFP/PEI_{25K} treatment (Fig. 7**B**).

3.8. *In vivo therapeutic efficacy*

Fig. 8**A** shows the in vivo antitumor activity of PMet-P($cdmPEG_{2K}$) micelles loaded with DOX alone, pIL-12 alone, and the combination of the two. Systemic delivery of DOX or pIL-12 via PMet-P($cdmPEG_{2K}$) micelles led to a modest antitumor activity. Co-delivery of the two led to a significant improvement in the antitumor activity. At 18 days post first injection, the tumor growth inhibition rates for pIL-12 micelleplexes, DOX-loaded micelles, and pIL-12/DOX co-loaded micelleplexes were 28.7%, 41.0% and 66.5%, respectively (Fig. 8C). Importantly, all the

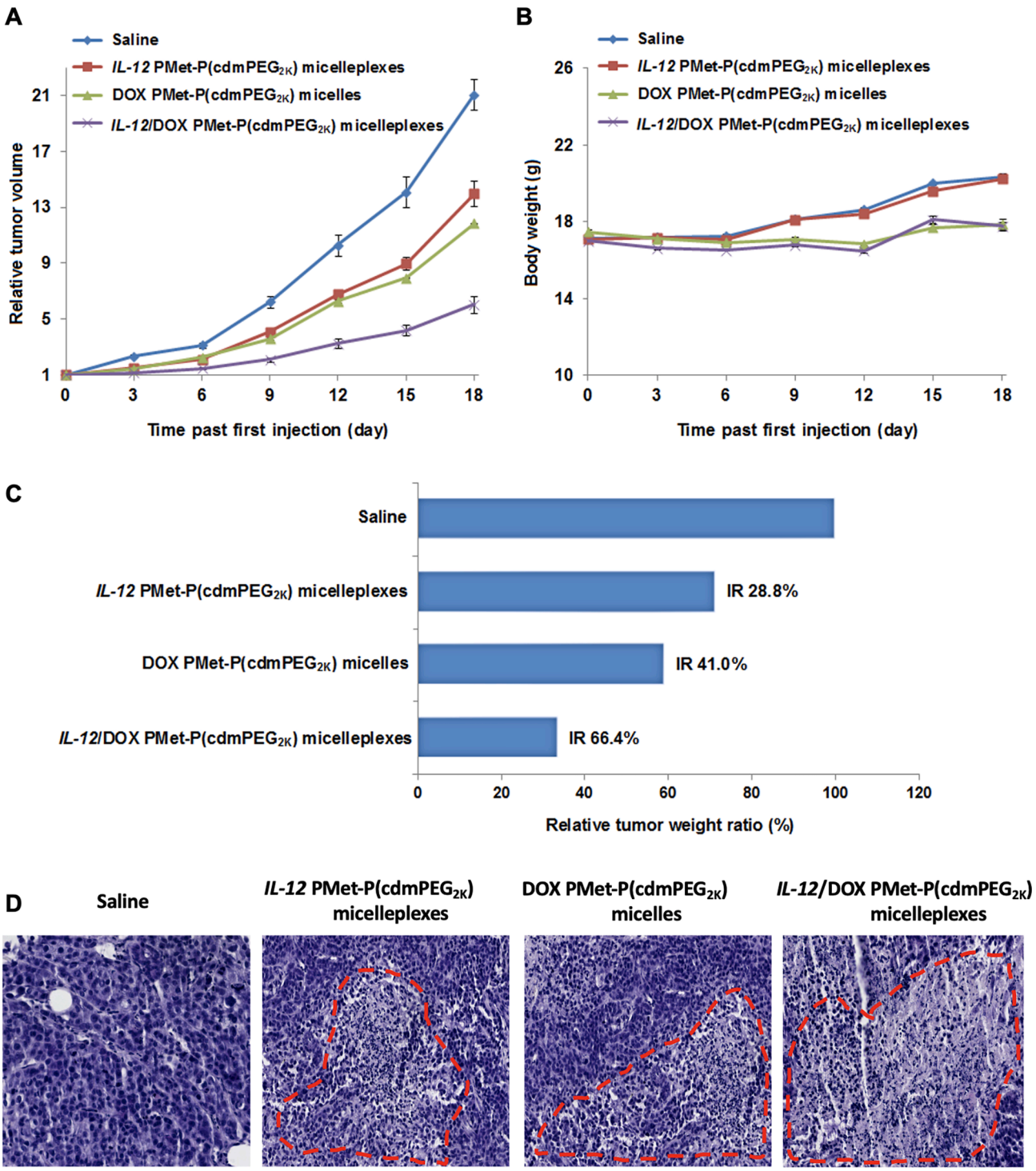

Fig. 8. In vivo therapeutic efficacy of *IL-12*/DOX co-loaded PMet-P(cdmPEG$_{2K}$) micelleplexes. (A) Tumor growth plotted as relative tumor volume (mean ± SEM, n = 5); (B) Body weight changes of mice in different treatment groups (mean ± SD, n = 5); (C) Tumor weights after excision, plotted as relative tumor weight ratio. Tumor growth inhibition rate (IR, %) was calculated as: (1- (mean tumor weight of drug treated group/mean tumor weight of saline treated group)) * 100%. (D) Histological analyses of tumor tissues collected on day 18 using H&E staining.

formulations were well-tolerated with normal increases in body weight during the observation period (Fig. 8B). Fig. 8D shows the pathohistological changes of tumors following different treatments. The tumors in saline-treated mice showed typical morphology of cancer cells with large nuclei. The tumor tissues in other treatment groups showed altered morphology with cell damage and shrunk nuclei. The group treated with pIL-12/DOX co-loaded micelleplexes exhibited the largest necrosis area, indicating that the best anti-tumor activity was seen with this co-delivery system.

The above results suggest that PMet-P(cdmPEG$_{2K}$) could be used as an intratumoral pH responsive carrier for effective co-delivery of pDNA and DOX to tumors for combination therapy.

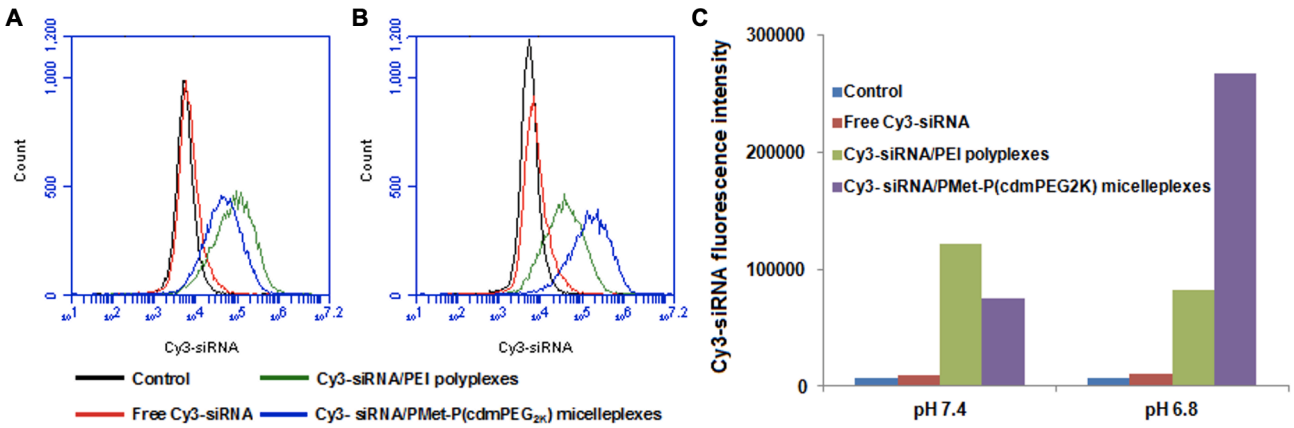

Fig. 9. Flow cytometry histograms of 4T1.2 cells after 4 h incubation with free Cy3-siRNA, Cy3-labeled siRNA/PEI_{25K} and Cy3-labeled siRNA/PMet-P($cdmPEG_{2K}$) micelleplexes in FBS-free culture medium at pH 7.4 (A) and pH 6.8 (B); Quantification of cell internalization of Cy3-siRNA-loaded polyplexes by mean fluorescence intensity (C). Negative control group was cells without any treatment.

3.9. Co-delivery of DOX and siRNA via the PMet-P(cdmPEG2K) micellar system

In addition to co-delivery of DOX and pDNA, we also evaluated if our PMet-P(cdmPEG2K) carrier could efficiently co-deliver DOX and small interfering RNA (siRNA) into tumors. First, the particle sizes of siRNA/PMet-P(cdmPEG2K) and siRNA/DOX co-loaded PMet-P(cdmPEG2K) micelleplexes were determined by DLS. Both micelleplexes showed small sizes of 70–80 nm, a size range that ensures effective targeting to tumors via the EPR effect.

The siRNA delivery efficiency of the PMet-P($cdmPEG_{2K}$) micelles was evaluated in 4T1.2 tumor cells by flow cytometry (Fig. 9). Compared with free Cy3-siRNA and Cy3-siRNA/PEI_{25K} polyplexes, the PMet-P($cdmPEG_{2K}$) micelles were significantly more effective at mediating intracellular delivery of siRNA to 4T1.2 cells, especially upon transfection under acidic conditions (pH 6.8).

To further investigate if the PMet-P($cdmPEG_{2K}$) carrier could simultaneously co-deliver DOX and siRNA into tumor cells, 4T1.2 tumor cells were treated with DOX/FAM-siRNA PMet-P($cdmPEG_{2K}$) micelleplexes and then similarly analyzed by CLSM. As shown in Fig. 10, cells treated with micelleplexes loaded with FAM-siRNA or DOX alone only showed the respective green fluorescence of FAM-siRNA and red fluorescence of DOX. However, both fluorescence signals were observed in cells treated with micelleplexes co-loaded with DOX and FAM-siRNA. DOX fluorescence signals were mainly observed in nuclei while the FAM-siRNA signals were largely found in the perinuclear region of cells. Importantly, DOX in the co-loaded micelleplexes was more effectively delivered to cells compared to micelleplexes loaded with DOX alone.

The in vivo siRNA delivery efficiency of PMet-P($cdmPEG_{2K}$) also was investigated in 4T1.2 tumor-bearing mice following intravenous injection of PMet-P($cdmPEG_{2K}$) micelleplexes carrying AF647-siRNA (Fig. 11). Strong fluorescence signals were detected in the tumor tissues at 6 h following i.v. injection and the signals remained in the tumors at 24 h post-injection. Significant levels of fluorescence were also found in spleen and liver due to the nonspecific uptake of the micelleplexes by reticuloendothelial system (RES). Only weak fluorescence signals were detected in heart and kidney. Collectively, these data suggest that the PMet-P($cdmPEG_{2K}$) carrier has the potential to effectively target delivery of nucleic acids including pDNA and siRNA for gene therapy.

4. Discussion

In our study, a metformin-based polymer PMet-P($cdmPEG_{2K}$) with a tumor extracellular pH-labile cdm linkage was developed for co-delivery of DOX and nucleic acids. The structure of the polymer was well characterized. It could form micelles at a low CMC value of 28.6 μg/mL, suggesting the favorable self-assembling behavior of PMet-P($cdmPEG_{2K}$) and excellent stability as a carrier after intravenous injection. The blank and DOX/PMet-P($cdmPEG_{2K}$) micelles showed an average size of 154 nm and 178 nm, respectively. They were able to efficiently condense pIL-12 into a more compact micelleplex structure with a smaller particle size of ~100 nm and a narrow size distribution. The more compact micelleplexes observed after complexation with pIL-12 might be due to the charge neutralization and non-covalent cross-linking of PMet-P($cdmPEG_{2K}$) micelles by pIL-12 [4].

PEGylation of micelles can minimize opsonin adhesion in blood, thus potentially prolonging the blood circulation time and increasing the tumor tissue accumulation via the EPR effect [40]. We found that the pIL-12/PMet-P(cdmPEG2K) micelleplexes showed higher serum stability than pIL-12/PEI25K polyplexes, due to the positive charge shielding effect of PEG on the PMet-P($cdmPEG_{2K}$) micellar surface. More importantly, the PEG shell was detachable from the pIL-12/DOX co-loaded PMet-P($cdmPEG_{2K}$) micelleplexes under lower pH, comparable to the pH in tumor microenvironment. This was demonstrated by the increases in the zeta potentials at pH 6.8 (29.8 mV) vs. pH 7.4 (10.7 mV). This is due to the cleavage of the cdm linker at the lower pH, leading to the re-exposure of the cationic amino groups on the surface of the micelleplexes. We hypothesize that the increase in positive charges in response to the lower pH facilitates the interaction with the negatively charged cell membrane, promoting the internalization of the micelles and improving both gene- and drug-mediated biological effect.

Interestingly, the release of DOX from the micelleplexes was much slower than that from micelles. This could be explained by the pIL-12 plasmid serving as a non-covalent cross-linker for the micelles, leading to more compact PMet-P($cdmPEG_{2K}$) micelleplexes. However, we didn't notice the increases in DOX release at pH 6.8 compared to pH 7.4, which might be due to only partial removal of the PEG shielding under the in vitro simulated condition. It is expected that the release will be significantly faster in vivo with the assistance of other disassembling and/or degrading mechanisms. Nonetheless, the sustained DOX release of DOX micelles and pIL-12/DOX co-loaded micelleplexes clearly indicate that the PMet-P($cdmPEG_{2K}$) micelleplexes experience minimal drug leaking during blood circulation, and take full advantage of the EPR effect to efficiently deliver chemotherapeutics and nucleic acids into tumor tissues.

It has been reported that the combination of cytotoxic drugs and immunostimulatory cytokines such as IL-12 provides a novel approach for cancer therapy [41–43]. However, systemic co-delivery of an *IL-12* encoding gene and DOX via intravenous injection for immunochemotherapy has not been explored previously. Our work shows that the PMet-P(cdmPEG2K) carrier can efficiently co-deliver a pIL-12 plasmid and DOX into tumors, and significantly improve the antitumor effect

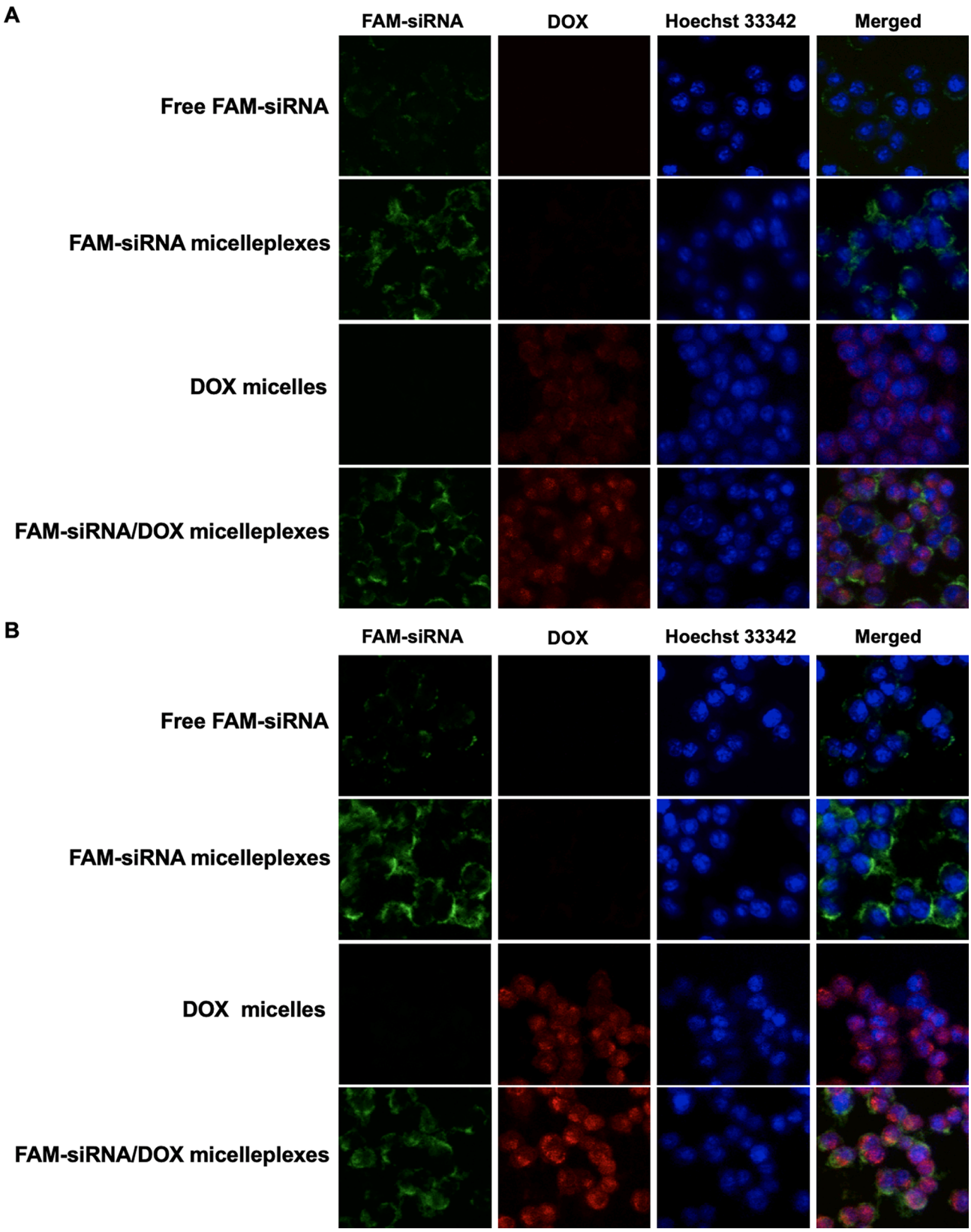

Fig. 10. CLSM of 4T1.2 cells after incubation with free FAM-labeled siRNA, DOX-loaded micelles, FAM-labeled siRNA loaded and *IL-12*/DOX co-loaded PMet-P (cdmPEG$_{2K}$) micelleplexes for 4 h in FBS-free culture medium at pH 7.4 (A) and pH 6.8 (B).

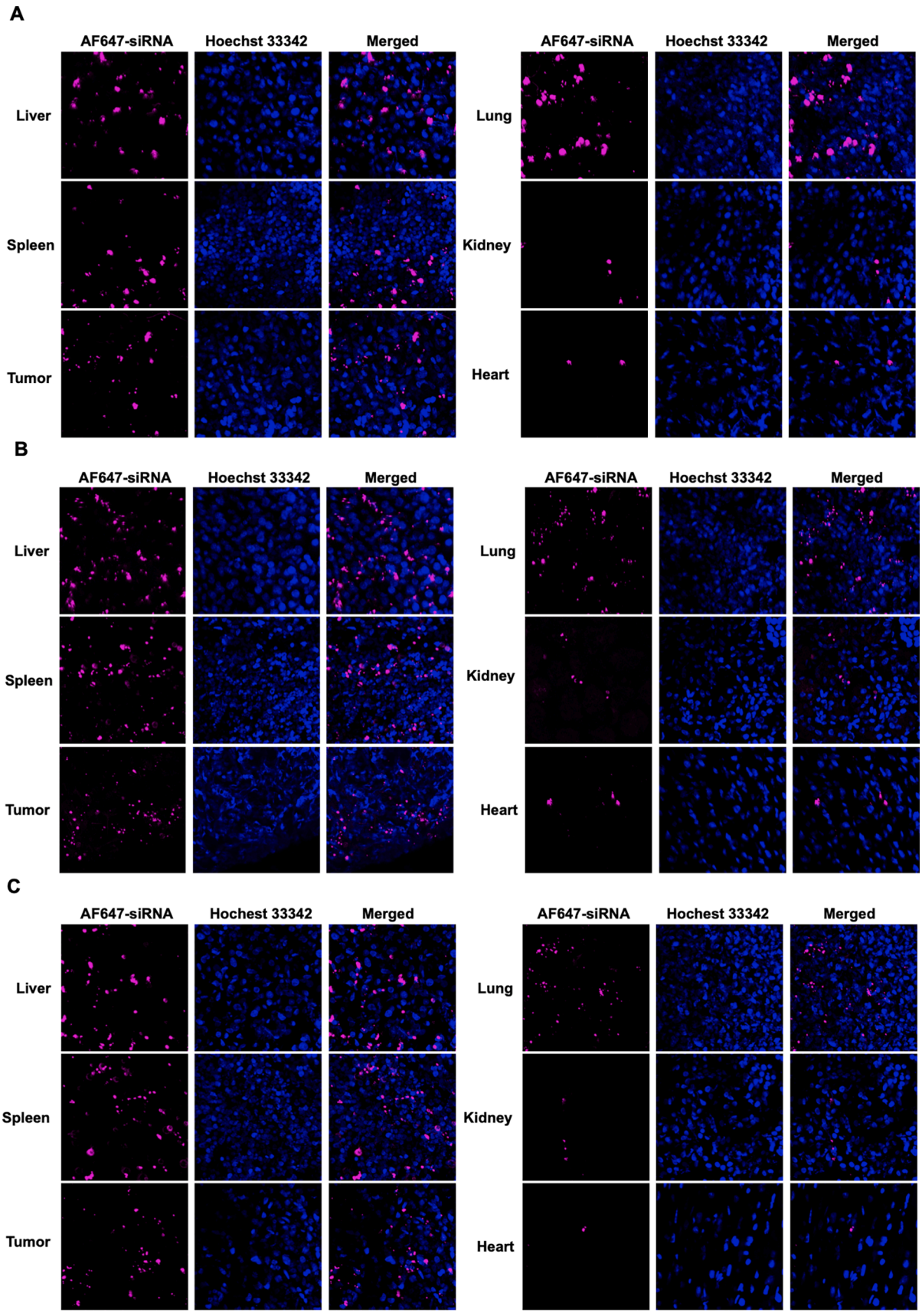

Fig. 11. Cryo-section of AF647-siRNA in tissues observed under CLSM after treatment with AF647-siRNA loaded PMet-P(cdmPEG$_{2K}$) micelleplexes for 6 (A), 16 (B) and 24 h (C) in 4T1.2 tumor-bearing mice.

compared to the PMet-P(cdmPEG2K) carrier loaded with pIL-12 or DOX alone. We hypothesize that the improved effect of the pIL-12/DOX co-loaded PMet-P(cdmPEG2K) is attributed to the synergy between pIL-12 and DOX [43]. The improved delivery of DOX may also be due to the more compact and stable structure of the co-loaded formulation.

Compared to the DOX/pDNA co-loaded PMet-P(cdmPEG2K) micelleplexes, the DOX/siRNA co-loaded micelleplexes showed a smaller particle size (~70 nm), which could be favorable for EPR-mediated tumor accumulation and the subsequent step of intracellular delivery via a particle size-dependent endocytosis pathway. Flow cytometry analysis demonstrated a higher level of siRNA delivery to 4T1.2 tumor cells for Cy3-siRNA/PMet-P(cdmPEG$_{2K}$) micelleplexes compared to free Cy3-siRNA and Cy3-siRNA/PEI$_{25K}$ polyplexes, especially upon transfection under acidic conditions (pH 6.8). This suggests that the pH responsive de-shielding property of the PMet-P(cdmPEG$_{2K}$) micelles can also facilitate the efficient siRNA delivery to tumor cells. Furthermore, the PMet-P(cdmPEG$_{2K}$) carrier also was able to co-deliver DOX and siRNA into tumor cells. DOX/siRNA co-loaded micelleplexes delivered more DOX to tumor cells compared to the micelleplexes loaded with DOX alone, likely due to a more stable structure of the co-loaded micelleplexes as a result of siRNA-mediated cross-linking of the micelleplexes. In vivo biodistribution data further confirmed that the PMet-P (cdmPEG$_{2K}$) carrier efficiently delivered siRNA into tumor tissues. In future, we will further evaluate the combination therapeutic efficacy of functional siRNA and chemotherapeutics co-delivered by the PMet-P (cdmPEG$_{2K}$) carrier.

In summary, a PMet-P(cdmPEG$_{2K}$) micellar system designed to lose the PEG shell under the more acidic extracellular tumor environment, was developed for efficient co-delivery of DOX and nucleic acids (pDNA/siRNA). The PEG layer of the PMet-P(cdmPEG$_{2K}$) micelleplexes was detached at pH = 6.8, resulting in the re-exposure of the positive charge of the micelleplexes thus promoting internalization of the micelleplexes by the tumor cells. The system demonstrates potent in vitro and in vivo gene delivery efficiency for the EGFP/luciferase reporter gene and siRNA. Co-delivery of a model gene *IL-12* and chemotherapeutic agent DOX through the PMet-P(cdmPEG$_{2K}$) micellar carrier showed an enhanced tumor therapeutic efficacy.

CRediT authorship contribution statement

Yanhua Liu: Conceptualization, Methodology, Formal analysis, Investigation, Writing - original draft. **Jingjing Sun:** Conceptualization, Methodology, Investigation, Writing - original draft. **Yixian Huang:** Conceptualization, Methodology, Investigation. **Yichao Chen:** Investigation. **Jiang Li:** Investigation. **Lei Liang:** Investigation. **Jieni Xu:** Investigation. **Zhuoya Wan:** Investigation. **Bei Zhang:** Investigation. **Zuojun Li:** Investigation. **Song Li:** Conceptualization, Methodology, Writing - original draft, Funding acquisition, Supervision, Project administration.

Declaration of Competing Interest

The authors declare that they have no known competing financial interests or personal relationships that could have appeared to influence the work reported in this paper.

Acknowledgment

This work was supported by National Institute of Health grants R01CA174305, R01CA219399, and R01CA223788. We would like to thank Dr. Robert Gibbs for editing our manuscript.

References

[1] E. Rheinbay, M.M. Nielsen, F. Abascal, J.A. Wala, O. Shapira, G. Tiao, H. Hornshøj, J.M. Hess, R.I. Juul, Z. Lin, Analyses of non-coding somatic drivers in 2,658 cancer whole genomes, Nature 578 (7793) (2020) 102–111.
[2] J. Kokkinos, R.M.C. Ignacio, G. Sharbeen, C. Boyer, E. Gonzales-Aloy, D. Goldstein, J.A. McCarroll, P.A. Phillips, A.P.C.G. Initiative, Targeting the undruggable in pancreatic cancer using nano-based gene silencing drugs, Biomaterials 240 (2020), 119742.
[3] M.M. Knott, T.L. Hölting, S. Ohmura, T. Kirchner, F. Cidre-Aranaz, T.G. Grünewald, Targeting the undruggable: exploiting neomorphic features of fusion oncoproteins in childhood sarcomas for innovative therapies, Cancer Metastasis Rev. 38 (4) (2019) 625–642.
[4] Y. Chen, J. Sun, Y. Huang, Y. Liu, L. Liang, D. Yang, B. Lu, S. Li, Targeted codelivery of doxorubicin and IL-36γ expression plasmid for an optimal chemo-gene combination therapy against cancer lung metastasis, Nanomed.: Nanotechnol. Biol. Med. 15 (1) (2019) 129–141.
[5] J. Sun, T. Luo, R. Sheng, H. Li, A. Cao, Preparation of cationic l-lysine conjugated poly (2-hydroxyethyl methacrylate) s and their potential application as low cytotoxic efficient gene delivery vectors, J. Control. Release 1 (172) (2013), e108.
[6] J. Sun, R. Sheng, T. Luo, Z. Wang, H. Li, A. Cao, Synthesis of diblock/statistical cationic glycopolymers with pendant galactose and lysine moieties: gene delivery application and intracellular behaviors, J. Mater. Chem. B 4 (27) (2016) 4696–4706.
[7] A. Aied, U. Greiser, A. Pandit, W. Wang, Polymer gene delivery: overcoming the obstacles, Drug Disc. Today 18 (21–22) (2013) 1090–1098.
[8] E.M. McErlean, C.M. McCrudden, H.O. McCarthy, Delivery of nucleic acids for cancer gene therapy: overcoming extra-and intra-cellular barriers, Therapeutic Deliv. 7 (9) (2016) 619–637.
[9] M. Mahato, G.R. Jayandharan, P.K. Vemula, Viral-and non-viral-based hybrid vectors for gene therapy, in: Gene and Cell Therapy: Biology and Applications, Springer, 2018, pp. 111–130.
[10] R. Yue, M. Chen, N. Ma, Dual MicroRNA-triggered drug release system for combined chemotherapy and gene therapy with logic operation, ACS Appl. Mater. Interfaces 12 (29) (2020) 32493–32502.
[11] C. Li, J. Hu, W. Li, G. Song, J. Shen, Combined bortezomib-based chemotherapy and p53 gene therapy using hollow mesoporous silica nanospheres for p53 mutant non-small cell lung cancer treatment, Biomater. Sci. 5 (1) (2017) 77–88.
[12] J.G. Fewell, M. Matar, J. Rice, D.H. Lewis, K. Anwer, Combination of immuno gene therapy and chemotherapy for treatment of cancer and hyperproliferative diseases, Google Patents, 2011.
[13] S. Uthaman, S. Maya, R. Jayakumar, C.-S. Cho, I.-K. Park, Carbohydrate-based nanogels as drug and gene delivery systems, J. Nanosci. Nanotechnol. 14 (1) (2014) 694–704.
[14] J. Xu, J. Sun, P.Y. Ho, Z. Luo, W. Ma, W. Zhao, S.B. Rathod, C.A. Fernandez, R. Venkataramanan, W. Xie, Creatine based polymer for codelivery of bioengineered MicroRNA and chemodrugs against breast cancer lung metastasis, Biomaterials 210 (2019) 25–40.
[15] C.-K. Chen, W.-C. Law, R. Aalinkeel, Y. Yu, B. Nair, J. Wu, S. Mahajan, J. L. Reynolds, Y. Li, C.K. Lai, Biodegradable cationic polymeric nanocapsules for overcoming multidrug resistance and enabling drug–gene co-delivery to cancer cells, Nanoscale 6 (3) (2014) 1567–1572.
[16] X. Wang, S.S. Liow, Q. Wu, C. Li, C. Owh, Z. Li, X.J. Loh, Y.L. Wu, Codelivery for paclitaxel and Bcl-2 conversion gene by PHB-PDMAEMA amphiphilic cationic copolymer for effective drug resistant cancer therapy, Macromol. Biosci. 17 (11) (2017) 1700186.
[17] L. Kang, Z. Gao, W. Huang, M. Jin, Q. Wang, Nanocarrier-mediated co-delivery of chemotherapeutic drugs and gene agents for cancer treatment, Acta Pharm. Sinica B 5 (3) (2015) 169–175.
[18] J. Chen, Z. Guo, H. Tian, X. Chen, Production and clinical development of nanoparticles for gene delivery, Mol. Therapy-Methods Clin. Develop. 3 (2016) 16023.
[19] T.S.C. Li, T. Yawata, K. Honke, Efficient siRNA delivery and tumor accumulation mediated by ionically cross-linked folic acid–poly (ethylene glycol)–chitosan oligosaccharide lactate nanoparticles: for the potential targeted ovarian cancer gene therapy, Eur. J. Pharm. Sci. 52 (2014) 48–61.
[20] G. Osman, J. Rodriguez, S.Y. Chan, J. Chisholm, G. Duncan, N. Kim, A.L. Tatler, K. M. Shakesheff, J. Hanes, J.S. Suk, PEGylated enhanced cell penetrating peptide nanoparticles for lung gene therapy, J. Control. Release 285 (2018) 35–45.
[21] J. Kim, Y. Kang, S.Y. Tzeng, J.J. Green, Synthesis and application of poly (ethylene glycol)-co-poly (β-amino ester) copolymers for small cell lung cancer gene therapy, Acta Biomater. 41 (2016) 293–301.
[22] G.Y. Liu, M. Li, C.S. Zhu, Q. Jin, Z.C. Zhang, J. Ji, Charge-conversional and pH-sensitive PEGylated polymeric micelles as efficient nanocarriers for drug delivery, Macromol. Biosci. 14 (9) (2014) 1280–1290.
[23] X. Yang, Q. Chen, J. Yang, S. Wu, J. Liu, Z. Li, D. Liu, X. Chen, Y. Qiu, Tumor-targeted accumulation of ligand-installed polymeric micelles influenced by surface PEGylation crowdedness, ACS Appl. Mater. Interfaces 9 (50) (2017) 44045–44052.
[24] M. Ramamoorth, A. Narvekar, Non viral vectors in gene therapy-an overview, J. Clin. Diagn. Res.: JCDR 9 (1) (2015) GE01.
[25] Z. Hu, X. Li, M. Yuan, X. Wang, Y. Zhang, W. Wang, Z. Yuan, Study on the effectiveness of ligand reversible shielding strategy in targeted delivery and tumor therapy, Acta Biomater. 83 (2019) 349–358.
[26] M. Tang, H. Dong, Y. Li, T. Ren, Harnessing the PEG-cleavable strategy to balance cytotoxicity, intracellular release and the therapeutic effect of dendrigraft poly-l-lysine for cancer gene therapy, J. Mater. Chem. B 4 (7) (2016) 1284–1295.

[27] J. Gao, Y. Xu, Y. Zheng, X. Wang, S. Li, G. Yan, J. Wang, R. Tang, pH-sensitive carboxymethyl chitosan hydrogels via acid-labile ortho ester linkage as an implantable drug delivery system, Carbohydr. Polym. 225 (2019), 115237.
[28] S.U. Kumar, V. Kumar, R. Priyadarshi, P. Gopinath, Y.S. Negi, pH-responsive prodrug nanoparticles based on xylan-curcumin conjugate for the efficient delivery of curcumin in cancer therapy, Carbohydr. Polym. 188 (2018) 252–259.
[29] W. Wu, L. Luo, Y. Wang, Q. Wu, H.-B. Dai, J.-S. Li, C. Durkan, N. Wang, G.-X. Wang, Endogenous pH-responsive nanoparticles with programmable size changes for targeted tumor therapy and imaging applications, Theranostics 8 (11) (2018) 3038.
[30] P. Jose, K. Sundar, C. Anjali, A. Ravindran, Metformin-loaded BSA nanoparticles in cancer therapy: a new perspective for an old antidiabetic drug, Cell Biochem. Biophys. 71 (2) (2015) 627–636.
[31] A. Luengo, L.B. Sullivan, M.G. Vander Heiden, Understanding the complex-I-ty of metformin action: limiting mitochondrial respiration to improve cancer therapy, BMC Biol. 12 (1) (2014) 1–4.
[32] M. Daugan, A.D. Wojcicki, B. d'Hayer, V. Boudy, Metformin: an anti-diabetic drug to fight cancer, Pharmacol. Res. 113 (2016) 675–685.
[33] C. Luo, L. Miao, Y. Zhao, S. Musetti, Y. Wang, K. Shi, L. Huang, A novel cationic lipid with intrinsic antitumor activity to facilitate gene therapy of TRAIL DNA, Biomaterials 102 (2016) 239–248.
[34] Y. Zhao, W. Wang, S. Guo, Y. Wang, L. Miao, Y. Xiong, L. Huang, PolyMetformin combines carrier and anticancer activities for in vivo siRNA delivery, Nat. Commun. 7 (1) (2016) 1–9.
[35] Z. Wan, J. Sun, J. Xu, P. Moharil, J. Chen, J. Xu, J. Zhu, J. Li, Y. Huang, P. Xu, Dual functional immunostimulatory polymeric prodrug carrier with pendent indoximod for enhanced cancer immunochemotherapy, Acta Biomater. 90 (2019) 300–313.
[36] H.-J. Li, J.-Z. Du, X.-J. Du, C.-F. Xu, C.-Y. Sun, H.-X. Wang, Z.-T. Cao, X.-Z. Yang, Y.-H. Zhu, S. Nie, Stimuli-responsive clustered nanoparticles for improved tumor penetration and therapeutic efficacy, Proc. Natl. Acad. Sci. 113 (15) (2016) 4164–4169.
[37] S. Gaali, C. Kozany, B. Hoogeland, M. Klein, F. Hausch, Facile synthesis of a fluorescent cyclosporin a analogue to study cyclophilin 40 and cyclophilin 18 ligands, ACS Med. Chem. Lett. 1 (9) (2010) 536–539.
[38] J. Sun, Y. Chen, J. Xu, X. Song, Z. Wan, Y. Du, W. Ma, X. Li, L. Zhang, S. Li, High Loading of hydrophobic and hydrophilic agents via small immunostimulatory carrier for enhanced tumor penetration and combinational therapy, Theranostics 10 (3) (2020) 1136.
[39] J. Jiang, S. Thayumanavan, Synthesis and characterization of amine-functionalized polystyrene nanoparticles, Macromolecules 38 (14) (2005) 5886–5891.
[40] J.S. Suk, Q. Xu, N. Kim, J. Hanes, L.M. Ensign, PEGylation as a strategy for improving nanoparticle-based drug and gene delivery, Adv Drug Deliv Rev 99 (Pt A) (2016) 28–51.
[41] J. Sun, Y. Chen, Y. Huang, W. Zhao, Y. Liu, R. Venkataramanan, B. Lu, S. Li, Programmable co-delivery of the immune checkpoint inhibitor NLG919 and chemotherapeutic doxorubicin via a redox-responsive immunostimulatory polymeric prodrug carrier, Acta Pharmacol. Sin. 38 (6) (2017) 823–834.
[42] J. Lu, X. Liu, Y.-P. Liao, X. Wang, A. Ahmed, W. Jiang, Y. Ji, H. Meng, A.E. Nel, Breast cancer chemo-immunotherapy through liposomal delivery of an immunogenic cell death stimulus plus interference in the IDO-1 pathway, ACS Nano 12 (11) (2018) 11041–11061.
[43] R.F. Little, K. Aleman, P. Kumar, K.M. Wyvill, J.M. Pluda, E. Read-Connole, V. Wang, S. Pittaluga, A.T. Catanzaro, S.M. Steinberg, Phase 2 study of pegylated liposomal doxorubicin in combination with interleukin-12 for AIDS-related Kaposi sarcoma, Blood 110 (13) (2007) 4165–4171.